Doubly differential secondary-electron yields following 8-MeV/u U^{68+}- and 3.5-MeV/u U^{38+}-ion impact on a thin carbon-foil target

D. Schneider, G. Schiwietz,* and D. DeWitt
High Temperature Physics Division, Lawrence Livermore National Laboratory, University of California, Livermore, California 94550
(Received 14 July 1992)

Doubly differential secondary-electron yields following the impact of 8-MeV/u U^{68+} and 3.5-MeV/u U^{38+} ions on 44-$\mu g/cm^2$ carbon-foil targets have been investigated experimentally. Electron emission yields were determined for ejection angles varied between 0° and 157° and electron energies ranging from 10 eV to 8 keV. The experimental data are compared to results from a theoretical model for production and transport of fast electrons in solids.

PACS number(s): 34.50.Fa

I. INTRODUCTION

Electron emission following the transmission of fast (MeV/u) heavy ions through thin foil targets has been the subject of several investigations in the past (e.g., Refs. [1–10], and references quoted therein). Recently new experimental data have been reported and are compared to newly developed theoretical model calculations [11]. The interest in a better understanding of the physical processes that are involved when highly charged ions transverse matter is diverse. The study of the secondary-electron emission from thin foil targets is of interest from both the fundamental and practical reasons. As demonstrated in a series of previous studies, experimental and theoretical investigations provide detailed information on the projectile energy-loss mechanisms. A considerable fraction of the projectile energy loss leads to the creation of high-energy electrons, which are predominantly emitted into the forward direction in the case of fast projectiles. Since the electron emission related strongly to the charge-state distribution of the projectile ion, information on the pre-equilibrium of charge-exchange and projectile-excitation processes can be deduced [10,11]. Measurements of doubly differential electron emission yields in particular are a sensitive test of model calculations and the understanding of the electron transport through the solid.

A good understanding of the dynamics of the electron emission by heavy-ion impacts is of value for practical reasons. There the nuclear track formation following the bombardment of fast (MeV/u) heavy ions with solids is of interest. The influence of the ion-induced track potential on the electron emission can elucidate the understanding of defects along the projectile path [12]. This is important for radiation physics [13,14], where high-energy heavy ions are used for radiotherapy. The proposed schemes for heavy-ion driven inertial confinement fusion require a detailed understanding of beam-pellet shell interactions and energy-loss mechanisms. Furthermore, these studies are of interest with regard to investigations of effects of cosmic rays on space-based computer systems [15]. Excited-state configurations in projectile ions undergoing ion-beam foil interactions have been studied using Auger-electron and competing x-ray emission spectroscopy (e.g., Ref. [16]). The corresponding intensities due to Auger-electron emission are superimposed on the secondary-electron continuum and contribute to the radiation-induced defects.

The general features of secondary-electron spectra following interactions of high-energy ions with gaseous targets have been described recently (e.g., Refs. [17,18]). The same general features and production mechanisms are present also in the case of foil targets. There, however, the electron transport through the solid is affected by their energy and angular straggling, which predominantly determines the electron emission in backward and forward angles. In addition, ion-induced track potentials, production of shock electrons as a result of collective excitations in the solid, plasmon excitation, and excitons are expected to determine the shape of the emission spectra for very low electron energies.

Here we studied the doubly differential electron emission yield for forward- and backward-emission angles. The highly charged fast uranium ions (8 MeV/u) lose their energy predominantly via ionization, which causes the production of rather intense electron emission spectra. The experimental doubly differential yields are compared with transport theoretical results and discussed.

II. EXPERIMENT

The experimental setup has been described previously in Ref. [18]. The 8-MeV/u U^{68+}-ion beams were produced at the Super HILAC (heavy-ion linear accelerator) of the Lawrence Berkeley Laboratory. Typical ion-beam currents of 5 to 10 nA were collimated to a spot size of about 2×2 mm^2 prior to entering the magnetically shielded scattering chamber. The normally-incident ion beam traverses the carbon foil in the center of the chamber and is collected in a Faraday cup. The secondary-electron emission was observed at different angles with respect to the ion-beam direction. The electron emission was analyzed by an electrostatic 90° parallel-plate analyzer with an intrinsic resolution of 8% (FWHM [full width at half maximum]), and a solid angle of 6×10^{-4} sr. The overall efficiency of the analyzer is about 0.3, including the efficiency of the electron multi-

plier, which has been determined from auxiliary measurements using gas targets [18]. The thickness of the carbon target was 44 $\mu g/cm^2$; the base pressure in the chamber was 3×10^{-7} Torr. The experimental data were normalized to the theory by fitting the data to the theoretical results at electron energies above 5 keV. In this energy regime, the theoretical data are expected to have uncertainties of the order of 30% [11]. The relative uncertainty with regard to variation of the emission angle is typically 15%.

III. THEORY

All theoretical results presented in this paper are based on classical transport theory. In order to avoid the statistical uncertainties of Monte Carlo solutions [4], the SELAS approximation (a separation of energy loss and angular scattering in the particle propagator function) was applied [11]. The corresponding transport equations are integrated for each initial state, ejection angle, and energy. This calculation requires the knowledge of the primary electron flux, which is obtained from semiempirical ion-atom collision cross sections. These cross sections, as well as the incorporated electron energy-loss cross sections, that account for plasmon excitations, are expected to be accurate for electron energies above about 30 eV. Channeling, blocking, and diffraction effects are expected to be of minor importance if other than single-crystalline materials are investigated. Furthermore, quantum-interference effects can be neglected, since many electrons are ejected per incident heavy ion and this leads to many (predominantly incoherent) final multielectron states. For a detailed description of the model, see Ref. [11].

Figure 1 displays theoretical electron ejection spectra for 8-MeV/u U^{68+} ions penetrating a 44-$\mu g/cm^2$ C-foil under normal incidence. The spectra were calculated for three ejection angles and three different electron production mechanisms: direct target and projectile ionization, as well as electron-electron collision cascades. Target ionization (upper part of Fig. 1) was computed for the 1*s*, 2*s*, and 2*p* shells separately for a projectile mean equilibrium charge state of $q=69$ [19]. Solid-state effects enter the calculation via the electron binding energies and the electron transport to the vacuum. Angular scattering and energy loss are of similar importance for the description of electron transport in dense matter. Both mechanisms yield a broadening of the spectral structures appearing in single-collision results. The energy loss leads to absorption of low-energy electrons from the initial electron flux. Hence, solid-state electron spectra, as displayed in the upper part of Fig. 1, show less variations as a function of the electron energy than the corresponding atomic spectra (see Refs. [17,18]). It is emphasized that the relative angular distribution of fast electrons differs also by orders of magnitude from atomic cross sections. This is due to the influence of multiple scattering, which is dominant for electrons ejected in backward directions.

The middle of Fig. 1 displays electron spectra due to ionization of populated projectile subshells by the neutral C target atoms. For the calculations, 21 electrons are assumed to be in the ground-state configuration and two electrons in Rydberg states distributed with $P_n=50/n^3$, where n is the orbital quantum number. The Rydberg-state population P_n was determined from a fit of calculated electron spectra to our experimental results. It is emphasized that the value of P_n is the only free parameter in the model calculation. In the present case, the fit depends only on the height of the pronounced δ-electron peak (the so-called convoy or cusp electrons) at 0°. This peak is mainly due to ionization of excited projectiles, the so-called electron loss into the projectile continuum (ELC), and corresponds to ejection of electrons centered around the projectile velocity (about 4400 eV at 0°). A possible cusp-peak contribution due to electron capture into the projectile continuum (ECC) is neglected in Fig. 1. At the charge-state equilibrium, the total electron-capture and electron-loss cross sections are equal [19]. Since the electron-capture process populates preferentially inner shells at high incident energies, the capture to the continuum is less than the bound-state capture cross section. Because this investigation was performed for incident charge states near the equilibrium, the ECC contribution to the cusp is expected to be of the order of 10%.

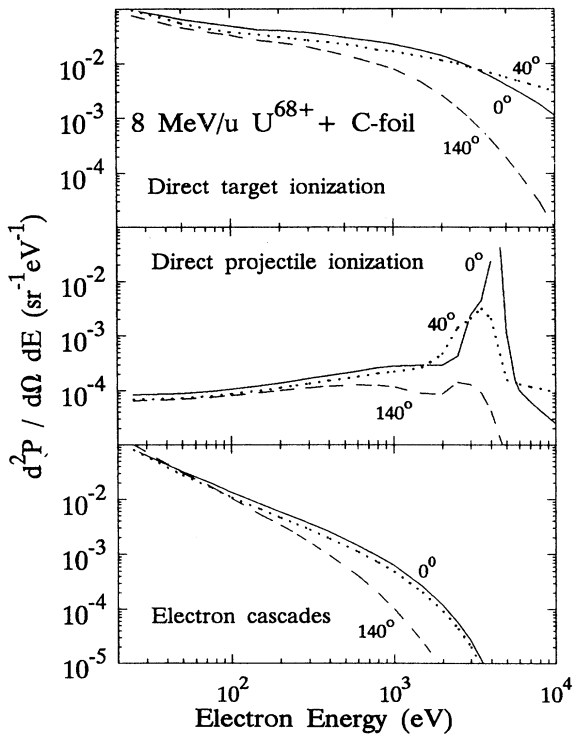

FIG. 1. Doubly differential electron emission yields calculated for three electron production mechanisms for 8-MeV/u U^{68+} impact on 44-$\mu g/cm^2$ carbon foils.

In a previous experiment, we have performed a direct measurement of the Rydberg yield using a field-ionization technique [20,8]. The corresponding result was $P_n=(210\pm40)/n^3$. The field-ionization technique is sensitive to n quantum numbers above 500, whereas the current fit is sensitive to quantum numbers in a range

around $n = 50$. Thus, the difference between both results is an indication of a deviation from the assumed n^{-3} dependence. The broad background in the projectile-electron spectra (see middle part of Fig. 1) is due to ionization of projectile inner-shell electrons and due to the slowing down of cusp electrons in the solid.

The lower part of Fig. 1 shows the calculated secondary-electron contribution from electron-electron collision cascades. A first generation of electrons is produced via direct projectile and target ionization (upper and middle part of Fig. 1). During the process of slowing down, these electrons ionize target atoms on their way and produce a second generation of electrons. The second produces a third electron generation, and so on. The sum of all electron generations, except for the first one, is denoted as the cascade contribution and shown in the lower part of Fig. 1. In practice, our calculation shows that the second- and third-generation electrons account for about 99% or more of this cascade electron flux at energies above 25 eV. Furthermore, it is emphasized that the significant cascade contribution is at electron energies below 100 eV.

IV. DISCUSSION OF RESULTS

Figure 2 displays the singly differential electron emission yields for 8-MeV/u U^{68+} and 3.5-MeV/u U^{38+} projectiles at forward (F) and backward (B) ejection angles. Experimental as well as theoretical emission yields (dashed lines) are integrated over the ejection angle in the corresponding hemisphere, leading to an uncertainty of $\pm 20\%$. The yields decrease over several orders of magnitude toward higher electron energies. In the experimental spectra, there is a structure at about 260 eV superimposed on the secondary-electron continuum. This structure is due to target K Auger-electron emission. For backward ejection, the yields decrease more rapidly as compared to the forward direction, and the C K Auger structure is observed more distinguished from the continuum. The theoretical δ-electron results are seen to agree well with the experimental data for backward ejection and for forward ejection at electron energies above 4000 eV. However, for slow electrons ejected in the forward direction, the discrepancy reaches a factor of 5. For strongly screened projectiles and nonequilibrium projectile charge states, the SELAS model gives only qualitative results. The corresponding data from 3.5-MeV/u U^{38+} ions incident on thin foil targets have been discussed previously in Ref. [21] on the basis of n-body classical trajectory Monte Carlo (n CTMC) calculations. In these calculations, the electron transport was benchmarked against experimental results for the angular and energy straggling of monoenergetic electrons incident on thin foils [22]. The data are shown for comparison here, and it is pointed out that two broad structures are visible in the forward direction for 3.5-MeV/u U^{38+} projectiles at about 4.5 keV and 7.6 keV electron energies. The broad peak at 4.5 keV corresponds to the binary-encounter peak expected for electron emission at 40°. These electrons are emitted near the projectile ions' exit from the foil, and they show the typical angular dependence expected for binary-encounter electrons. The peak and shoulder at 7.6 keV is due to binary electrons initially scattered to 0° deep inside the solid. These "hot" electrons undergo subsequently large-angle scattering with small average energy loss. They cause a peak at an electron energy expected for binary electrons emitted into 0°, and they do not shift with observation angle. This double binary-encounter peak structure is well reproduced in model calculations using the n CTMC method [21].

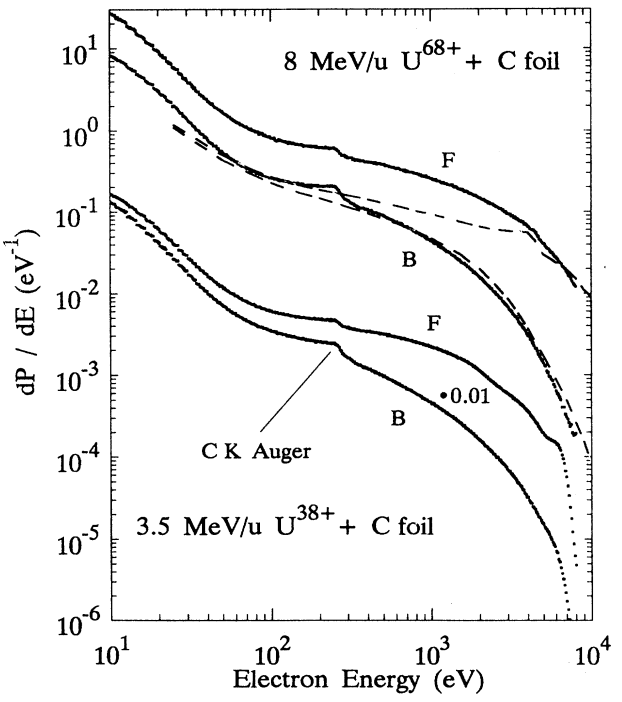

FIG. 2. Singly differential electron emission yields for forward (F) and backward (B) ejection following 8-MeV/u U^{68+} and 3.5-MeV/u U^{38+} impact on 44-$\mu g/cm^2$ and 20-$\mu g/cm^2$ carbon foils, respectively.

Table I shows the mean electron energies and ejection yields for secondary electrons and Auger electrons derived from Fig. 2. The uncertainties stated in the table include statistical uncertainties and the effect of the extrapolation of the spectra to zero energy (20% relative uncertainty) and to the binary-encounter peak. It is noted that about 2000 electrons are ejected per incident projectile for 8-MeV/u U ions. For comparison, data taken previously for fast Ne projectiles [11] have been partly reevaluated using the current uranium data for interpolation purposes and displayed in the table. The mean energies are identical for Ne and U ions of the same speed to within the experimental uncertainties. The total electron yields scale with the square of the mean equilibrium charge state [19], as predicted by first-order perturbation theory. However, the Auger-electron yield is only 1% of the total yield for U ions, whereas it is 4% for Ne ions. At present, it is not clear whether surface contaminations or the ion-induced track potential [12] are responsible for this deviation. For uranium ions, the high ionization density in the track could, in principle, lead to reduced

TABLE I. Total electron emission yields (P), corresponding mean electron energies (E), and Auger-electron yields (A) for U and Ne ions incident on carbon foils of thickness t. The subscripts F and B correspond to the fractions being emitted in forward and backward directions, respectively.

Projectile	t (μg/cm^2)	E_F (eV)	E_B (eV)	P_F	P_B	A_F	A_B
3.5-MeV/u U^{38+}	44	820±50	240±30	1300±500	630±250	8.3±4	6.5±3
8.0-MeV/u U^{68+}	44	880±60	300±40	2000±800	470±200	16.1±8	9.8±5
3.5-MeV/u Ne^{10+}	20	750±70	200±60	26[a]	10[a]	0.76[a]	0.42[a]
8.5-MeV/u Ne^{7+}	100	1100±200	400±100	16±3	6.2±1.5	0.61±0.15	0.32±0.08

[a]Relative values normalized to $P_B = 10$.

recombination rates. For the (mainly) highly ionized target atoms, this will result also in reduced Auger yields, if the recombination time is on the order of the optical lifetimes. The measured forward-backward asymmetry with respect to Auger-electron emission is mainly due to secondary-electron induced K-shell ionization [9].

Figures 3 and 4 show doubly differential electron emission yields for 8-MeV/u U^{68+} projectiles penetrating a 44-μ/cm^2 C foil. Theoretical electron emission yields are displayed for 120°, 140°, and 160° in the backward direction and for 0°, 20°, 40°, and 60° in the forward direction. These yields correspond to the sum of the three secondary-electron contributions shown in Fig. 1. The spectral structures are similar to the singly differential spectra in Fig. 2, except for 0°, where the cusp peak is visible. At backward angles, the deviation between experiment and theory is an effect of the SELAS approximation. Fast electrons detected in the backward direction are predominantly produced deep inside the solid. Initially, most of them fly in the forward direction and undergo a few large-angle scattering events, until they are emitted at the backside of the foil (this is the most important reason for the solid-state–gas-phase differences in the angular distribution of ejected electrons). In such cases, the electron path lengths inside the solid, and the corresponding energy loss, depend strongly on the number of angular-scattering events. Thus, a separation of energy loss and angular scatterings (the SELAS approximation) is hardly possible for fast electrons ejected in the backward direction. As estimate for the variation of the

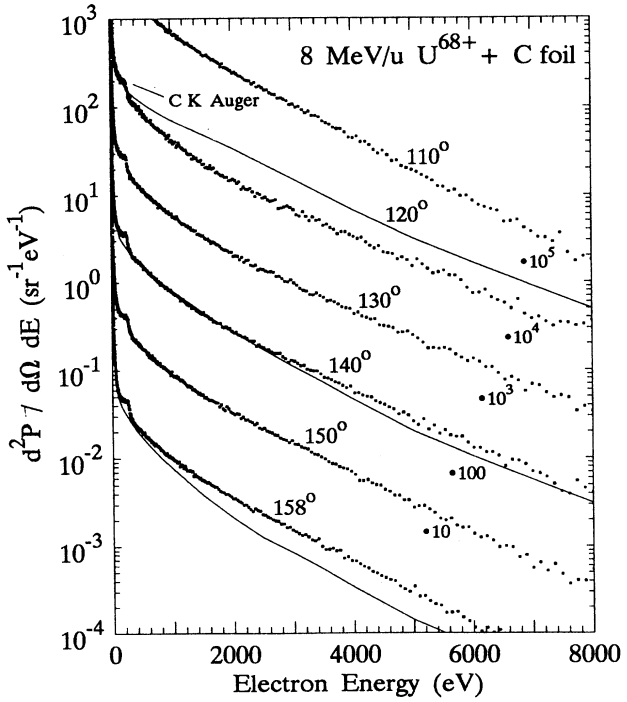

FIG. 3. Doubly differential electron emission yield in backward direction following 8-MeV/u U^{68+}-ion impact on 44-μg/cm^2 carbon foils.

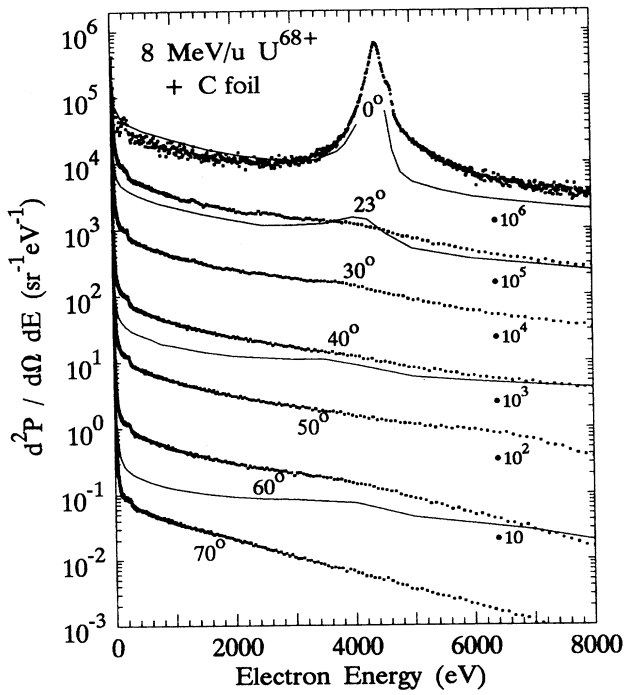

FIG. 4. Doubly differential electron emission yields in forward direction following 8-MeV/u U^{68+}-ion impact on 44-μg/cm^2 carbon foils.

electron path length due to plural scattering shows: (i) the SELAS results (using a straight-line path length) should underestimate the experimental data at 180° and high electron energies by a factor of about 2, and (ii) the predicted angular distribution of ejected electrons should be more pronounced than the experimental one. Both statements are in agreement with the results presented in Fig. 3.

For small forward ejection angles, there is reasonable agreement between theory and experiment. At 0°, the measured "convoy" peak consists partly (shoulder and wing on high-energy side) also of electrons due to field ionization of highly excited Rydberg ions in the electrostatic spectrometer field [8]. It is noted that the shape and intensity of this peak depends on the type of 0° spectrometer. For larger angles, the model predicts a broadened cusp peak (due to energy loss and angular scattering) at energies below 4400 eV, whereas our experimental data do not show a significant structure at these energies. Moreover, at large forward angles (40° and 60°), the deviation between calculated and measured data reaches a factor of 6 at low electron energies. Similar deviations at large forward angles below the cusp energy were already found in a previous investigation with fast highly charged Ne ions [11]. It was speculated that the high ionization density along the ion tracks leads to an enhancement of forward ejected electrons, which are slightly slower than the projectile. However, for U^{68+} projectiles, such an effect should be significantly larger than for Ne^{10+} ions. Since this is not the case, the deviation at 60° is probably independent of the projectile atomic number. A possible reason for this failure of our model might again be the use of the straight-line approximation for the average path length l. The straight-line path length for an electron starting at a distance x from a surface is $l=|x/\cos\theta|$, where θ is the electron detection angle. In reality, this path length also depends on the initial direction inside the solid, and especially those electrons that are produced with velocity vectors parallel to the surface will have a strongly increased average path length. Such electrons will preferentially be observed at angles near 90°, and their average energy will be lower than for other ejection angles.

In summary, doubly differential electron yields have been deduced for electron energies in the range of 10 eV to 8 keV and ejection angles between 0° and 160° in 8-MeV/u U^{68+}- and 3.5-MeV/u U^{38+}-ion impact on 44-$\mu g/cm^2$ carbon-foil targets. The results are discussed on the basis of calculated emission yields, applying classical transport theory for electrons traversing the foil target. A Rydberg-state population of $P_n=50/n^3$ could be extracted from a fit of the theoretical electron-loss contribution to the experimental data. Furthermore, the model allows for an identification of the different electron production mechanisms in the electron spectra. However, the poor agreement between calculated and measured spectra at low energies and ejection angles near 90° indicates the need for improved model calculations. It is an open question which of the current electron-transport models [3,4,11,21] is best suited for an accurate prediction of doubly differential electron emission yields in the case of fast incident ions. Each of them seems to have problems in the treatment of either low-energy electron ejection [21,11] or fast incident particles [3,4]. It is emphasized that the measured spectra correspond to a yield of about 2000 ejected electrons per incident ion. This number is in accord with other results for the specific yield of carbon [2] and with data taken previously for Ne ions when scaled with the squared equilibrium projectile charge. It is not clear, at present, why the Auger-electron yield measured in this work is lower than predicted on the basis of this scaling.

ACKNOWLEDGMENTS

The authors are grateful for the provision of the high-quality charged uranium ion beams at the LBL Super HILAC facility. This work has been performed under the auspices of the Department of Energy by the Lawrence Livermore National Laboratory under Contract No. W-7405-ENG-48. We are also grateful to L. Ferrand for her assistance during the experiments.

*Permanent address: Hahn-Meitner-Institute, Department P, Glienicker Str. 100, 1000 Berlin 39, Germany.

[1] R. A. Baragiola, P. Ziem, and N. Stolterfoht, J. Phys. B **9**, L477 (1976).

[2] D. Hasselkamp, H. Rothard, K. O. Groeneveld, J. Kemmler, P. Varga, and H. Winter, in *Particle Induced Electron Emission II,* edited by G. Höhler, E. A. Niekisch, and J. Treusch, Springer Tracts in Modern Physics Vol. 123 (Springer, Heidelberg, 1991).

[3] M. Rösler and W. Brauer, *Particle Induced Electron Emission I,* edited by G. Höhler, Springer Tracts in Modern Physics Vol. 122 (Springer, Berlin 1991).

[4] L. H. Toburen, W. E. Wilson, and H. G. Paretzke, Phys. Rev. B **25**, 713 (1982).

[5] D. Schneider, N. Stolterfoht, D. Ridder, H. C. Werner, R. J. Fortner, and D. L. Matthews, IEEE Trans. Nucl. Sci. **NS-26**, 1136 (1979); D. Schneider, R. Kudo, and E. Kanter, Nucl. Instrum. Methods B **10**, 113 (1985).

[6] K. O. Groeneveld, R. Mann, W. Meckbach, and R. Spohr, Vacuum **25**, 9 (1974).

[7] R. E. Pferdekämpfer and H. G. Clerc, Z. Phys. **1275**, 223 (1975).

[8] G. Schiwietz, D. Schneider, and J. Tanis, Phys. Rev. Lett. **53**, 1567 (1987).

[9] G. Schiwietz, D. Schneider, J. P. Biersack, N. Stolterfoht, D. Fink, A. Mattis, B. Skogvall, H. Altevogt, V. Montemayor, and U. Stettner, Phys. Rev. Lett. **61**, 2677 (1988).

[10] H. Rothard, J. Schou, and K. O. Groeneveld, Phys. Rev. A **45**, 1701 (1992).

[11] G. Schiwietz, J. P. Biersack, D. Schneider, N. Stolterfoht, D. Fink, V. J. Montemayor, and B. Skogvall, Phys. Rev. B **41**, 6262 (1990); G. Schiwietz, Radia. Eff. Defects Solids **112**, 135 (1990).

[12] G. Schiwietz, P. L. Grande, B. Skogvall, J. P. Biersack, R. Köhrbrück, K. Sommer, A. Schmoldt, P. Goppelt, I. Kadar, S. Ricz, and U. Stettner, Phys. Rev. Lett. **69**, 628

(1992).
[13] L. H. Toburen, N. F. Metting, and L. A. Brady, Nucl. Instrum. Methods B **40/41**, 1275 (1989).
[14] G. Kraft, Nucl. Sci. Appl. **3**, 1 (1987).
[15] P. V. Dressendorfer, Nucl. Instrum. Methods B **40/41**, 1291 (1989).
[16] E. Martinson, Nucl. Instrum. Methods B **43**, 323 (1989).
[17] N. Stolterfoht, D. Schneider, J. Tanis, H. Altevogt, A. Salin, P. D. Fainstein, R. Rivarola, J. P. Grandin, J. H. Audriamonje, D. Bertault, and J. Chemin, Euro. Phys. Lett. **4**, (8), 899 (1987).
[18] D. Schneider, D. DeWitt, A. S. Schlachter, R. E. Olson, W. G. Graham, J. R. Mowat, R. D. Dubois, D. H. Loyd, V. Montemayor, and G. Schiwietz, Phys. Rev. A **40**, 2971 (1989).
[19] H. D. Betz, Rev. Mod. Phys. **44**, 465 (1972); V. S. Nikolaev and I. S. Dmitriev, Phys. Lett. **28A**, 277 (1968).
[20] D. Schneider, Nucl. Instrum. Methods B **24/25**, 173 (1987); J. Molitoris and D. Schneider, Lawrence Livermore National Laboratory Report No. UCRL-JC-105941, 1990.
[21] R. A. Sparrow, R. E. Olson, and D. Schneider, J. Phys. B **25**, L295 (1992).
[22] S. Lencinas, J. Burgdörfer, J. Kemmler, O. Heil, K. Kroneberger, N. Keller, H. Rothard, and K. O. Groeneveld, Phys. Rev. A **41**, 1435 (1990).